

Improving the age constraints on the archeological record in Scladina Cave (Belgium): new speleothem U-Th ages.

Hubert B. Vonhof¹, Sophie Verheyden², Dominique Bonjean³, Stéphane Pirson^{4,5}, Michael Weber⁶, Denis Scholz⁶, John Hellstrom⁷, Hai Cheng^{8,9}, Xue Jia⁸, Kevin Di Modica³, Gregory Abrams^{10,3}, Marjan A.P. van Nunen¹¹, Joost Ruiter¹¹, Michèle van der Does¹², Daniel Böhl⁶, and H. Jeroen L. van der Lubbe¹¹

¹Max Planck Institute for Chemistry, Mainz, Germany

²Royal Belgian Institute of Natural Sciences, Brussels, Belgium

¹⁰³Scladina Cave Archaeological Centre, Espace muséal d'Andenne, Andenne, Belgium

⁴Wallonia Heritage Agency, Scientific and Technical Direction, Namur, Belgium

⁵University of Liège, Department of Geology and European Archaeometry Centre, Liège, Belgium

⁶Johannes Gutenberg University, Institute for Geosciences, Mainz, Germany

⁷University of Melbourne, Melbourne, Australia

¹⁵⁸Institute of Global Environmental Change, Xi'an Jiaotong University, Xi'an 710054, China

⁹Institute of Earth Environment, Chinese Academy of Sciences, Xi'an 710061, China

¹⁰ArcheOS – Research Laboratory for Biological Anthropology, Department of Archaeology, Ghent University, Ghent, Belgium

¹¹Vrije Universiteit Amsterdam, Institute of Earth Sciences, Amsterdam, the Netherlands

²⁰¹²Alfred Wegener Institute, Helmholtz Centre for Polar and Marine Research, Bremerhaven, Germany.

Correspondence to: Hubert B. Vonhof (Hubert.vonhof@mpic.de)

Abstract. The sedimentary sequence in Scladina Cave (Belgium) is well-known for its rich Middle Paleolithic assemblages and its numerous faunal remains. Of particular interest is the presence of a nearly complete mandible of a Neandertal child.
25 To place all these finds in the correct chronostratigraphic context, various dating techniques have been applied over the past decades. This resulted in a reasonably well-constrained age model, roughly spanning the last glacial cycle. Age constraints of the lower part of the Scladina sequence as well as from the underlying Sous-Saint-Paul Cave were however absent until now. Previous attempts to date several speleothem layers in Scladina Cave, using U-Th dating were only partly successful, presumably because diagenetic alteration of speleothem material compromised the ages. In the present study we re-assessed
30 U-Th dating of various speleothem levels in Scladina Cave, applying state-of-the-art U-Th dating, and carefully selecting material that experienced little to no diagenetic alteration. The new results constitute a robust age framework for the Scladina sequence, which provides precisely dated stratigraphic anchor points that improve the previous age model. Furthermore, new U-Th analyses, for speleothems from the lower part of the Scladina sequence and from the Sous-Saint-Paul sequence, document Middle Pleistocene ages, making this one of the longer fossil-rich cave sedimentary sequences in NW Europe. The new data
35 confirm that speleothem growth predominantly took place in periods of warmer climate, while siliciclastic sediments

characterize the colder intervals. New speleothem ages further suggest that the Neandertal mandible found in the sequence, and previously placed in Marine Isotope Stage 5a or 5b, could potentially be as old as Marine Isotope Stage 5d.

1 Introduction

40 Scladina Cave is situated near the Belgian town Sclayn in a valley branching off the Meuse River (Fig. 1). The cave has been investigated since 1971, following the discovery of Middle Palaeolithic artefacts at the entrance of the cave (Bonjean et al., 2014). The cave at that time was nearly completely filled with a stack of siliciclastic sediments and intercalated flowstone levels. After several decades of careful scientific excavation, a significant part of the sedimentary infill has been excavated (Fig. 2), and the cave continues to deliver a wealth of archaeological and paleontological information (Bonjean et al., 2014).
45 Arguably the most significant fossils retrieved from the cave are the mandible, a fragment of right maxillary and sixteen teeth of a juvenile Neandertal (Bonjean et al., 1996; Otte et al., 1993; Toussaint and Bonjean, 2014). Owing to careful excavation methods and favourable conditions for the preservation of ancient DNA in Scladina Cave, it has been possible to extract valuable genomic information from the mandible (Orlando et al., 2006; Peyregne et al., 2019). Besides this Neandertal material, a wealth of artefacts (stone tools) and fossil faunal remains have been retrieved from the sedimentological sequence in the
50 cave (Bonjean et al., 2014; Otte, 1992), and geochemical analyses on that material have provided valuable insight in the paleoenvironmental and palaeoecological setting (Bocherens et al., 1997; Bocherens, 2014).

The chronostratigraphic context of the finds from the cave has been reconstructed using a variety of dating techniques, anchored in meticulous reconstruction of the lithostratigraphy and sedimentary dynamics (Bonjean, 1998; Pirson, 2007, 2014; Pirson et al., 2014b; Pirson et al., 2008). The dating technique that is often most reliable in cave settings, Uranium series dating
55 of speleothem CaCO_3 , however, did not yield very precise ages initially (Bonjean, 1998; Gewelt et al., 1992). Presumably this was due to diagenetic alteration of speleothem calcite, as most speleothem material has been buried in siliciclastic sediments in Scladina Cave, and degradation of speleothem calcite is commonly observed in the excavated material.

Summarizing all the dating efforts done so far, a consistent age model is available for the spatially complex Scladina Cave infill stratigraphy (Pirson, 2014; Pirson et al., 2014b). In that age model, flowstone levels separating the different siliciclastic
60 stratigraphic units generally seem to represent the warmer climate periods through the last glacial cycles, as is also the case in other caves in Belgium (Quinif, 2006). However, the accuracy of the existing age model for Scladina has not been easy to establish, as the dating methods used have significant uncertainties, some parts of the sedimentary infill are difficult to date and some discrepancies between age estimates remain (Pirson et al., 2014b). Furthermore, the age model of the lower part of the sequence, including the sediments in the underlying Sous-Saint-Paul Cave is essentially unknown.
65 In the present paper, we have reinvestigated the potential for Uranium series dating of speleothem material in Scladina Cave. This is done because significant progress has been made in U-Th dating of speleothem material over the past decades. Particularly the advent of Multi-Collector Inductively Coupled Plasma Mass Spectrometry (MC-ICP-MS) has enabled more

precise analysis of U and Th on smaller samples than previously possible (Cheng et al., 2013; Scholz and Hoffmann, 2008). Furthermore, new and better-preserved speleothem material has been excavated from the cave. The objective of this study was
70 to carefully select the best-preserved flowstone and stalagmite material in the cave. In doing so, we targeted all known speleothem levels that were thick enough to preserve good quality speleothem calcite. We included two flowstone levels from the Sous-Saint-Paul Cave, the sediments of which stratigraphically underlie Scladina Cave (Otte, 1992; Pirson et al., 2008). In addition to our dating efforts, we used laser ablation ICP-MS elemental analysis on the speleothem material to characterize the diagenetic state of the material.

75 **2 Materials and methods**

2.1 Speleothem sample collection

The current stratigraphic profile of the sediment infill of Scladina Cave, including the sediments from the underlying Sous-
80 Saint-Paul Cave, is shown in Fig. 3. It contains several levels with speleothem material, the most prominent of which are the currently still active speleothems growing on top of unit H. From this level we collected 2 stalagmites and a column for analysis. A single speleothem was collected from layer 1B-BK (in unit 1B-BRUN). Two more stalagmites were collected from another prominent speleothem growth interval in unit 4A, previously dated to marine isotope stage (MIS) 5: one is coming from an in-situ speleothem (CC4 in unit 4A-IP), while the other one consists of two halves of a stalagmite reworked from CC4
85 in a gully (unit 4A-CHE). From a speleothem complex in stratigraphic unit 6B, we collected two stalagmites, and from two more speleothem levels in Sous-Saint-Paul Cave, covering the lowermost part of the composite sequence, we cut flowstone fragments. Slabs prepared from the samples collected, are shown in Fig. A1. Standard petrographic thin sections of selected samples were cut and polished from these slabs.

90 **2.2 U-series analysis**

$^{230}\text{Th}/\text{U}$ -dating of the selected material was performed over a period of several years in four different laboratories. In all laboratories, samples were dissolved in nitric acid before adding a mixed ^{229}Th - ^{233}U - ^{236}U spike solution and separating U and Th using ion exchange columns. The spike solutions were independently calibrated in the corresponding laboratories. The
95 analyses were performed by MC-ICP-MS, but with different instruments in the individual laboratories.

At Xi'An Jiaotong University, China, U and Th were co-precipitated using a Fe solution and subsequently extracted using an anion exchange resin (BioRad AG 1-X8) to extract Th and U, respectively. The final solution was analysed on a Thermo Fisher

Scientific Neptune Plus MC-ICP-MS. The entire procedure was carried out at the Institute of Global Environmental Change, Xi'an Jiaotong University (China) and followed established protocols (e.g. Cheng et al., 2020).

100 At the University of Melbourne, Australia, sample preparation and chemical separation of U and Th and MC-ICP-MS measurements followed established protocols (Hellstrom, 2003). The equilibrated and spiked solution was loaded onto an ion exchange column containing Eichrom TRU and pre-filter resin to discard the calcite matrix and finally elute U and Th. The U-Th fractions were analysed on a Nu Instruments Plasma MC-ICP-MS at the University of Melbourne (e.g. Weij et al., 2024).

105 At the Max Planck Institute for Chemistry (MPIC), Mainz, Germany, U and Th were separated from the spiked sample solution using ion exchange column chemistry (Yang et al., 2015) and analysed using a Nu Instruments Plasma MC-ICP-MS (Obert et al., 2016).

At the Institute for Geosciences, Johannes Gutenberg University (JGU), Mainz, Germany, samples were passed through ion exchange columns filled with 1.5 mL of Bio-Rad AG 1-X8 anion exchange resin to separate U and Th. Mass spectrometric 110 analyses of U and Th (cf Obert et al., 2016) were conducted using a Thermo Fisher Scientific Neptune Plus MC-ICP-MS.

All activity ratios and ages were calculated using the half-lives reported by Cheng et al. (2013) and corrected for detrital contamination assuming a $^{232}\text{Th}/^{238}\text{U}$ weight ratio of 3.8 for the detritus and ^{230}Th , ^{234}U and ^{238}U in secular equilibrium (Wedepohl, 1995). To account for the uncertainty of the correction, we assumed an uncertainty of 50 %, which was fully 115 propagated to the corrected activity ratios and ages. All uncertainties are reported at the 2σ -level.

2.3 Stable isotope analysis of CaCO_3

Samples were analysed on a Thermo Delta-V mass spectrometer at MPIC Mainz equipped with a Gasbench II preparation

120 device. ~8-50 microgram of CaCO_3 sample, placed in a He-filled 12 ml exetainer vial, were digested in >99% H_3PO_4 . Subsequently the CO_2 -He gas mixture was transported to the Gasbench in 5.0-grade Helium carrier gas. In the Gasbench, water vapor and various gaseous compounds were separated from the He- CO_2 mixture prior to sending it to the mass spectrometer for isotope analysis, and reported as $\text{CaCO}_3 \delta^{13}\text{C}$ ($\delta^{13}\text{C}_{\text{cc}}$) and $\text{CaCO}_3 \delta^{18}\text{O}$ ($\delta^{18}\text{O}_{\text{cc}}$) on the “Vienna PeeDee Belemnite” (VPDB) scale.

125 The In-house CaCO_3 standard VICS (having a $\delta^{13}\text{C}$ value of 1.45‰ VPDB and a $\delta^{18}\text{O}$ value of -5.44‰ VPDB) was analyzed with each run of samples. CaCO_3 standard weights of standards are chosen so that they span the entire range of sample weights of the samples. After correction of isotope effects related to sample size the reproducibility of the standards typically is better than 0.1 ‰ (1SD) for $\delta^{18}\text{O}$ and 0.1 ‰ (1SD) for $\delta^{13}\text{C}$.

130 2.4 Stable isotope analysis of dripwater

A single dripwater sample from Scladina Cave taken on 5 July 2010 was analysed by use of a Thermo TC-EA pyrolysis furnace coupled to a Delta XP mass spectrometer at Vrije Universiteit Amsterdam (VU). Analytical precision (1SD) of 4 in-house water standards (8 repetitive analyses for each) in the sample series that contained this sample did not exceed 0.2 ‰ $\delta^{18}\text{O}$ and 1.0 ‰ for $\delta^2\text{H}$. Triplicate analysis of the sample itself resulted in a 1SD precision smaller than that of the standard water reproducibility. Isotope data of the dripwater sample is reported on the “Vienna Standard Mean Ocean Water” (VSMOW) scale.

140 2.5 Fluid inclusion isotope analysis

140

Fluid inclusion isotope analyses were performed on discrete ~ 0.5-1.0 g chips of speleothem calcite, cut from the speleothem slabs using a Dremel microdrill with diamond-lined rotary drill blade. These samples were crushed under a controlled atmosphere in a crushing cell attached to a Picarro L2140*i* water isotope analyser at the Max Planck Institute for Chemistry in Mainz, Germany. The resulting hydrogen and oxygen isotope values of fluid inclusion water ($\delta^2\text{H}_{\text{fi}}$ and $\delta^{18}\text{O}_{\text{fi}}$ respectively) are 145 reported on the VSMOW scale. Typical 1SD precisions for this technique, based on standard water injections in this system, are better than 0.3 ‰ for $\delta^{18}\text{O}_{\text{fi}}$ values and 1.0 ‰ for $\delta^2\text{H}_{\text{fi}}$ values (De Graaf et al., 2020).

150 2.6 Laser ablation trace element analysis

150 Trace element concentrations were measured by laser ablation ICP-MS at the MPIC following the procedure of Jochum et al. (2012), with a high-resolution sector-field ICP-MS ThermoElement2, interfaced with a New Wave UP-213 Nd:YAG laser ablation system. The silicate glass NIST SRM 612 was analysed for external calibration of the trace element analyses. Data are reported in $\mu\text{g/g}$ (ppm) units.

155 3 Results

3.1 Cave site and regional climate

The mean annual surface temperature in the nearby town of Andenne is ~10.4 degrees Celsius and average monthly
160 temperatures typically range between 3 and 18 degrees Celsius (KMI, 2024). Cave temperature monitoring from July 2010
until July 2011 showed an annual cycle between 8 and 13 degrees C, with an average annual value of 10.5 degrees C, which
is dampened in seasonality, but very close to the mean annual surface temperature of the region. Based on accounts of the
archeological staff on site, drip rates in the cave are variable, depending on rainfall amounts above the cave. This likely relates
to the small hydrological catchment area of Scladina Cave (see Fig. 1). Relative humidity measurements in the cave taken at
165 different points in time typically were close to 100%.

3.2 Diagenetic screening of speleothem samples

170 The thinner speleothem layers, present in the cave sediments, commonly appear significantly altered, which is macroscopically
evidenced by yellow and brownish discolorations, and sometimes even loss of the original “brittle” nature of the calcite. Such
altered samples have become much softer than pristine speleothem calcite from this site. In contrast, the more prominent
speleothem layers, particularly when developed in stalagmite morphology, appear visually much better-preserved.
175 Stalagmites growing from the top of unit H (specimens 2010#1, 2010#2 and 2012#5) appear overall well preserved,
presumably because they represent the only material that has not been covered by siliciclastic sediments.

Speleothems collected from under unit H have all been buried in siliciclastic sediments. These speleothems often show
discolorations on the outer surface of such stalagmites, that look much alike those of the poorly preserved material from the
thinner layers. For some specimens, like 2014#618, the discolorations appear on the inside of the speleothem as well, but
generally closer to the surface that had been exposed to the siliciclastic sediment. In all stalagmite material we took subsamples
180 from near the growth axis, avoiding visible discolorations, and targeting areas that showed clear lamination that we interpreted
to be the original calcite fabric. Thin section observations from several of these samples reveal columnar fabrics (Fig. 4), which
are generally taken to represent unaltered speleothem calcite (Frisia et al., 2000), suggesting that this sampling strategy indeed
selects the well-preserved material. One thin section of a sample that seemed less well-preserved, (2012#6) shows fine
microsparite (Fig 4), which is considered to point towards diagenetic recrystallisation. That sample was removed from the
185 dataset before further analysis.

Two flow stones from the Sous-Saint-Paul cave (2012#3 and 2012#4) were sampled along the central axis of the sample we
took, and show columnar calcite fabrics (Fig 4).

The effect of diagenetic alteration on speleothem material that was buried in siliciclastic sediments in the cave was geochemically characterized in a laser ablation ICP-MS transect measured at high spatial resolution from the visually well-preserved core of stalagmite 2014#618 (unit 6B) to its diagenetically altered outer surface (Fig. 5). The transect in total is 42 mm long. Whitish and yellowish discoloration, black irregular laminae, and loss of visible lamination and transparency towards the more altered zone near the outer surface of the speleothem suggest diagenetic alteration upon macroscopic inspection. Calcite fabric at the growth axis lacks these features, and macroscopically looks unaltered.

Clearly shown in the trace element data is that ^{238}U and ^{232}Th have high concentrations at the outer surface of the stalagmite, that has been in direct contact with the sediment in which it was buried. ^{238}U shows a gradient of decreasing values towards the core of the speleothem, reaching stable $\sim 0.1\text{ppm}$ concentrations in the central growth axis of the speleothem which represents the CaCO_3 material that appears unaltered at visual inspection. This gradient is much sharper for ^{232}Th , which shows markedly increased values only at the outer surface of the stalagmite.

Elements like Strontium and Phosphorus show patterns very comparable to that of ^{238}U . In contrast, the Mn distribution does not compare well to that of ^{238}U , nor to ^{232}Th .

Please note that single scattered datapoints towards higher values, best visible in the ^{88}Sr and ^{232}Th traces in Fig. 5 are considered to be analytical artefacts (outliers) occurring during laser ablation.

3.3 U-Th ages

205

The results of U-Th dating are presented in Table 1 and Fig. 6. The speleothems from unit H, all yield Holocene ages, which generally confirms previously published U-Th ages of this unit (Gewelt et al., 1992). The stratigraphically oldest sample from the base of stalagmite 2012#5 from that speleothem complex, reaches 8.9 ka, and the ages of the composite record of stalagmites on top of unit H seem to suggest near-continuous speleothem growth until the present day.

210 Stalagmite 2014#206 from layer 1B-BK (unit 1B-BRUN) produced four ages (Table 1). Two of which, at the base of the stalagmite, indicate growth in MIS-5a and another two higher up in the stalagmite correspond to MIS-3 (Fig. 6). Comparatively little stalagmite growth thickness between these two age clusters may suggest reduced or no growth in MIS-4.

Unit 4A stalagmites yield consistent ages, that all fit in MIS-5e, the warmest stage of MIS-5 (Table 1; Fig. 6). The oldest ages we captured for unit 4A are 121 ka. The youngest age for the two unit-4A stalagmites analysed is 116 ka.

215 Two stalagmites from flowstone levels in stratigraphic unit 6B yield ages at 197 ka for specimen 2014#618, and ages from 142 to 174 ka for specimen 2010#6. The older ages can be attributed to the warm period MIS-7a, which fits the general pattern that, in Scladina Cave, speleothems grew predominantly during interglacials. Interestingly, the younger age range of specimen 2010#6 places it in MIS-6, which is a glacial period.

The next speleothem level further down in the Scladina Cave stratigraphy, is in fact situated in the underlying Sous-Saint-Paul Cave, in unit XVII, which is connected to Scladina cave by an open vertical shaft near the entrance of the cave. For the sub-

samples taken from flowstone sample 2012#4 we have consistent ages of 300-311 ka at ± 9 ka 2σ uncertainties, suggesting the flowstone formed under interglacial conditions in MIS-9 (Fig. 6; Table 1).

The lowest speleothem level encountered in the Sous-Saint-Paul Cave (2012#3) again is a flowstone layer, related to unit XIX. For this layer the ages plot between 363 and 536 ka (Table 1), measured in three labs, roughly spanning the time period between 225 MIS-14 and MIS-10. The ages are partly inverted, which is perhaps not surprising in view of the high and variable dating uncertainties (from 105 to 14 ka at 2σ level) in a time interval that is so close to the limit of what can still be dated with the U-Th technique. In any case, the ages of Sous-Saint-Paul Cave suggest that its sedimentary infill predates that of Scladina cave.

230

3.4 Fluid inclusion stable isotope data

235 For all specimens studied we performed isotope analysis of fluid inclusion water on multiple subsamples. The isotope composition of fluid inclusion water in speleothem calcite ($\delta^2\text{H}_{\text{fi}}$ and $\delta^{18}\text{O}_{\text{fi}}$) is considered to represent that of the drip water in the cave at the time of speleothem growth, which in turn is a direct proxy for the isotope composition of (paleo)rainfall recharging the cave aquifer (Dennis et al., 2001; Van Breukelen et al., 2008). The oldest specimen, 2012#3, contained too little fluid inclusion water for analysis. Fluid inclusion isotope values from most other speleothems, presented in Table 2 and Fig.

240 7, fall on a trend with part of the samples plotting around an endmember close to the Global Meteoric Water Line (GMWL). Part of the data trend away from the GMWL at a relatively low angle towards higher $\delta^2\text{H}_{\text{fi}}$ and $\delta^{18}\text{O}_{\text{fi}}$ values (Fig. 7). This trend seems to occur in data from all studied time intervals, with one clear exception. This exception is specimen 2012#4, dated at MIS 9 age, that displays the lowest $\delta^2\text{H}_{\text{fi}}$ and $\delta^{18}\text{O}_{\text{fi}}$ data of all material analysed and plots in a tightly constrained field close to the GMWL (Fig. 7).

245 The fluid inclusion isotope data that plot near the GMWL have isotope values close to the annually-averaged isotope composition of modern regional rainwater ($\delta^2\text{H}_{\text{p}}$ and $\delta^{18}\text{O}_{\text{p}}$), of -47.3 and -6.8 ‰ (VSMOW) for $\delta^2\text{H}$ and $\delta^{18}\text{O}$ respectively. Rainfall data is provided by the Global Network of Isotopes in Precipitation (IAEA/WMO, 2023) database for the Liege Weather station (for the years 1966-1970). A single drip water sample from Scladina Cave (taken on July 5, 2010) gave a $\delta^2\text{H}$ value of -42.4 ‰ and a $\delta^{18}\text{O}$ value of -6.5 ‰, which is also close to the weighted-average rainfall isotope values for Liege, as 250 documented in the Global Network of Isotopes in Precipitation database.

4 Discussion

4.1 Diagenetic screening of the samples

255 While there is no doubt that diagenesis has at least partly altered the Scladina Cave speleothems, we have made several observations indicating that diagenesis is not pervasive, and that in the samples we selected for U-Th analysis we successfully avoided diagenetically altered parts of the speleothems. Particularly the Laser Ablation ICP-MS trace element patterns (Fig. 5) suggest significant diagenetic alteration on the stalagmite outer surface, while the calcite in the growth axis shows trace element concentrations that fit unaltered speleothem calcite. The different gradients of ^{238}U and ^{232}Th from the diagenetic 260 surface towards the unaltered growth axis are interpreted to reflect the contrasting solution chemistry of U and Th. U can move in dissolved form with diagenetic fluids into the speleothem, while the less soluble Th, stays behind in particulate or colloidal state, on the outside. Elements like Strontium, also readily mobile in solution, show very comparable concentration trends to Uranium, suggesting that, once buried in detrital cave sediments, a dissolution-reprecipitation diagenetic front penetrated into the speleothems from the surface inwards, altering trace element patterns.

265 Diagenetic alteration of speleothem calcite is described in several earlier studies, and different diagenetic processes have been suggested. Commonly observed is the post depositional transition from aragonite to calcite fabrics (Frisia, 2015 and references therein), which is a process we do not believe to be of significance for the present study, as we find no evidence for aragonite mineralogy in our material. Another process is redissolution of speleothem material due to changing dripwater chemistry, which may lead to recrystallisation along the stalagmite growth axis (Scholz et al., 2014). Further, neomorphism, or “cryptic” 270 diagenesis has been reported for stalagmites (Bajo et al., 2016; Frisia, 2015) which is often seen as fine scale infiltration of water in speleothems accompanied by thin-film dissolution - reprecipitation reactions capable of affecting the geochemical composition of speleothems, without clearly visible changes to the texture of the calcite. The latter process has been suggested to be able to affect U-Th ages (Bajo et al., 2016).

The diagenetic patterns that we observe in the trace element data seems to be in line with such neomorphic processes. Also, 275 the less commonly-observed elevated phosphorous content, that lines up well with diagenetic increase of U and Sr, likely result from mobilisation of bat guano phosphate present in the detrital sediment matrix, and subsequent diagenetic precipitation in the speleothem calcite fabric (Audra et al., 2021).

For the present study, the most important observation is that well before the transect reaches the growth axis of the speleothem, the trace element concentrations stabilize at values which are typical of well-preserved speleothem calcite. It appears therefore 280 that the speleothem calcite we selected for U-Th analysis is sufficiently well-preserved to yield good radiometric ages.

One more observation that follows from the trace element data is that the black laminae, occurring in some of the specimens studied, contain Manganese. These Manganese enrichments do not line up with the diagenetic patterns in Sr, U, and P. If these

Mn enrichments are diagenetic, it appears that they are not formed by the same diagenetic process. In any case, we stayed away from these dark laminae when sampling for U-Th analysis.

285 This careful diagenetic screening of speleothem samples has led to what appears to be a relatively consistent U-Th chronology of the Scladina speleothem sequence. When properly applying ^{232}Th corrections and considering the analytical uncertainties that result from that, no age reversals are present in the dataset, with the exception of the samples from the oldest flowstone level 2012#3, which are very close to the dating limit of the U-Th technique. Where different specimens from a single stalagmite horizon were analysed, the resulting ages appear generally consistent, also between the different labs where the
290 dating took place.

4.2 Fluid inclusion isotope ratios

In “low water-rock ratio” systems like speleothem calcite and its fluid inclusions, diagenetic alteration is expected to impact

295 the fluid inclusion isotope composition more readily than it will impact the calcite (Uemura et al., 2020).

Still, about half of fluid inclusion isotope data in Fig. 7 plots close to the GMWL, which suggests that these isotope data still represent the original rainwater values. This is corroborated by the relatively good comparison of these fluid inclusion isotope data to modern dripwater and rainwater isotope values from the area. The observation that another sub-set of the fluid inclusions trend away from the GMWL (Fig. 7), resembles a case of diffusive water loss from speleothem calcite, reported as

300 being the result of an analytical artefact in a recent study by Fernandez et al. (2023). Fernandez and co-workers describe how sample heating prior to isotope analysis in fluid inclusion isotope instrumentation can lead to partial water loss from fluid inclusions, because the host mineral loses sealing capacity under higher temperatures. Such partial water loss leads to isotope fractionation of the remaining water. While in the study by Fernandez et al. (2023) diagenesis did not play a role, we postulate that, in the case of Scladina Cave, diagenetic alteration may have contributed to the weakening of the fluid inclusion sealing
305 capacity, leading to isotope fractionation very similar to what Fernandez et al. (2023) describe. Thus, the fluid inclusion isotope data of diagenetically compromised samples are more likely to plot away from the GMWL. This seems to be supported by the observation that two samples, taken from the most altered parts of stalagmite 2014#618-3 (Table 2), lost so much of their water in the warm-up stage already (presumably because of diagenetic weakening of fluid inclusion sealing), that they could not be analysed anymore.

310 We next combined the oxygen isotope composition of the fluid inclusions ($\delta^{18}\text{O}_{\text{fi}}$) with that of the corresponding host calcite ($\delta^{18}\text{O}_{\text{c}}$), to calculate past cave temperatures based on the assumption of 1) isotope equilibrium during formation, and 2) absence of post-depositional alteration of fluid inclusion water or calcite (Table 2). Based on a widely accepted calculation specifically made for speleothems (Tremaine et al., 2011), these data show that fluid inclusion isotope values plotting further away from the GMWL lead to unrealistically high temperatures (Fig. B1), which supports that these fluid inclusion isotope values indeed
315 were no longer original when they were measured. Most of the data plotting close to the GMWL, however, result in

paleotemperatures in the range of the modern (interglacial) cave temperatures, suggesting, in good agreement with the observations by (Fernandez et al., 2023), that these fluid inclusion and calcite isotope values are essentially unaltered, and provide what we interpret to be the original rainwater isotope values during formation of the speleothems.

320 4.3 Paleoclimatological backdrop of speleothem growth in Scladina Cave

Based on the robust age framework for the horizons of speleothem growth in Scladina Cave it is now possible to consider the paleoclimatological backdrop of speleothem growth at this site in more detail than previously possible. Alignment of the 325 Scladina speleothem ages along the late Quaternary Probabilistic Benthic Stack (Ahn et al. 2017) confirms that speleothem growth in Scladina Cave generally took place during Interglacial periods. (Fig. 6). During Glacial periods, sedimentation in Scladina Cave was dominated by siliciclastic influx (Pirson et al., 2014b).

Ages for the oldest speleothem (flowstone) material in this record have higher age uncertainties, and can therewith not be tied to a single interglacial period. All we can say is that growth occurred in the time period from MIS-10 to MIS-14 based on the U-Th data we collected for these older samples.

330 Finally, two speleothems have ages that suggest deposition in non-interglacial conditions. Stalagmite 2010#6 has U-Th ages ranging from 174 ka to 142 ka, which corresponds to Glacial period MIS-6, and stalagmite 2014#206 has ages of ~78-74 ka at the base (corresponding to MIS-5a), and ages around 53 ka towards the top (corresponding to MIS-3). For stalagmite 2010#6, growth of particularly the older part of this specimen coincided with wetter conditions in Southern Europe, and the well-documented Mediterranean Sapropel S6 event that relates to a maximum in Northern hemisphere summer insolation (Bard et

335 al., 2002; Kroon et al., 1998; Sancho et al., 2015; Wainer et al., 2013). Stalagmite 2010#6 may suggest that these wet conditions occurred further North in Europe as well. Even though Western Europe and the Mediterranean region experienced relatively wet conditions at that time, global sea level was significantly below the modern values (Bard et al., 2002). This appears to indicate that speleothem growth in Scladina Cave did not necessarily require full interglacial settings in the past. Favourable hydrological conditions around 170-174 ka could perhaps relate to comparatively high sea surface temperatures (SST's) at the

340 Iberian margin at that point in time (Martrat et al., 2007). At 142 ka, the youngest age of stalagmite 2010#6 coincides with some of the lowest temperatures in MIS 6. Iberian margin SST's are also low, coinciding with the maximum ice extent in Northern Europe (Ahn et al., 2017). While we cannot discard this U-Th analysis on analytical grounds, this remains an age that we regard with some caution. Growth conditions for speleothems in Scladina Cave must have been rather unfavourable at 142 ka, and we are also not aware of other speleothem occurrences of this age in Northern Europe.

345 Stalagmite 2014#206 is another specimen that grew under non-interglacial conditions. It has ages of ~78-74 ka at the base (corresponding to MIS-5a), and ages around 53 ka towards the top (corresponding to MIS-3).

This interval is characterized by millennial-scale Dansgaard Oeschger variability (Rasmussen et al., 2014), which is well documented in Greenland Ice cores, whereby Greenland interstadials (warmer periods) would likely have been more

350 favourable than Greenland stadials (colder periods) for speleothem growth in Scladina Cave. The oldest ages of 2014#206
350 correspond to the time interval of Greenland interstadial GI-21, and Greenland stadial GS-20; (Rasmussen et al., 2014), and
the younger ages of 2014#206 correspond to pronounced Greenland interstadial GI-14. (Fig. 6). Regardless of their assignment
355 to Greenland stadials or interstadials, all measured ages of speleothem 2014#206 correspond to relatively high SST's at the
Iberian margin, that are to some extent decoupled from Dansgaard Oeschger variability recorded in the NGRIP ice core for
this time interval (Martrat et al., 2007). Particularly the interval around 53 ka also corresponds to a clear peak in tree pollen,
355 and other forest indicators in the Eifel Maar record (Riechelmann et al., 2023). For both intervals around 76 ka and 53 ka,
speleothem growth occurred at several other European sites (Lechleitner et al., 2018; Peral et al., 2024; Riechelmann et al.,
2023).

360 4.4 New U-Th ages in comparison to the existing Scladina Cave age model

The new ages we present here compare favourably to the existing age model of Scladina Cave (Fig. 8; Pirson et al., 2014b).
Methodological progress made over the past decades clearly comes forward in the direct comparison to previously published
365 U-Th ages (Bonjean, 1998; Gewelt et al., 1992) that are generally in the same range as our ages, but with much larger
uncertainties. Because we have more precise ages now, and provided ages in previously undated intervals, our data allow for
several changes and additions to the existing age model.

First, the ages we provide for the lower part of the Scladina stratigraphic sequence chart new territory. The oldest units in the
Scladina Cave sequence that we could date are from a speleothem complex in unit 6B. At an age of 197 ka, these speleothems
correlate to the latest part of MIS-7, while it has previously been systematically positioned inside MIS 5 (Bastin, 1992;
370 Bonjean, 1998; Cordy and Bastin, 1992; Pirson et al., 2014b). These new ages demonstrate that the older part of the Scladina
sequence belongs to the Middle Pleistocene, and more specifically to the Late Saalian.

Furthermore, the ages of the unit 4A-IP stalagmites unequivocally indicate that they grew in MIS-5e, equivalent to the Eemian
period (Shackleton et al., 2003), while in the previous age model, these were attributed to MIS-5a or MIS-5c (Pirson et al.,
375 2014b). This has implications for the currently accepted age of the Scladina 1-4A Juvenile Neandertal remains, as these were
found in a unit directly overlying this stalagmitic floor. Even though the reworked nature of the Neandertal fossils (Pirson et
al., 2014a) as well as the lack of precision in the chronology of the sequence situated immediately above unit 4A-IP (Pirson,
2014) prevent firm conclusions, the new ages make it more plausible that the deposition of the Neandertal remains predate
MIS-5a, and more probably belong to MIS 5d.

These ages further suggest that the Middle Palaeolithic assemblage from unit 5 (Bonjean et al., 2014), that so far was dated at
380 130 ± 20 ka (Huxtable and Aitken, 1992) and positioned inside MIS-5 (Pirson et al., 2014b), predates MIS-5e. If we would
choose to reject the 142 ka age in the top section of speleothem 2010#6 from unit 5B, on the grounds that speleothem growth

would have been rather unlikely in the glacial conditions that prevailed at that time, then the Middle Palaeolithic assemblage from unit 5 postdates the brief climate amelioration dated at 170-174 ka in MIS-6 (as recorded in the two older ages from stalagmite 2010#6). The stratigraphical placement of the unit 5 archaeological assemblage in MIS-6 (Fig. 3) is then also in
385 good agreement with the Infrared-stimulated Luminescence (IRSL) derived age of 153 ± 15 ka obtained from unit 4B, overlying unit 5 (Pirson et al., 2014b). If the 142 ka age of the top of stalagmite 2010#6 is taken to be accurate, however, then the unit 5 Paleolithic assemblage would most likely have been deposited in the last and coldest part of MIS 6.

Finally, our results allow, for the first time, to assign ages to the stratigraphy of the underlying Sous-Saint-Paul Cave, showing
390 that this sequence developed during the Middle Pleistocene. Adding the sedimentary record of the underlying Sous-Saint-Paul Cave to that of Scladina Cave extends the complete sedimentary sequence down to at least MIS-10 or perhaps even to MIS-14, which makes this one of the stratigraphically longer cave sedimentary records in North-West Europe.

5 Conclusions

395 In Scladina Cave, and in the underlying Sous Saint Paul Cave, burial of speleothems in siliciclastic sediments deposited in glacial periods has led to diagenetic alteration of speleothem calcite. Neomorphic alteration from the speleothem surface inwards, leads to visible discolourations, and is shown in trace element patterns. In the diagenetic process, observed mobilisation of ^{238}U , compromises U-Th dating of altered material. In the same process, PO_4 , likely sourced from bat guano in the sediment, was mobilised and remineralised in the speleothem fabric. Still, the diagenetic process was not pervasive, and through careful
400 sample screening we identified speleothem material with little to no diagenetic alteration from Sous-Saint-Paul and Scladina Caves, for U-Th dating. U-Th ages of these well-preserved speleothems confirm that their formation in these two connected caves predominantly occurred in warm (interglacial or interstadial) periods of the late Quaternary. Intercalated siliciclastic sediments were the dominant mode of deposition in colder periods. The data provide a robust age framework for Scladina Cave, and add precisely dated stratigraphic anchor points to the younger part of the sequence, that improve the previous age
405 model. One notable consequence of the new U-Th ages is that a juvenile Neandertal mandible, previously placed in Marine Isotope Stage 5a or 5b, could now potentially date back to Marine Isotope Stage 5d. Furthermore, new U-Th analyses, provide Middle Pleistocene ages for the previously undated lower part of the Scladina sequence, and the underlying Sous-Saint-Paul sequence. All ages combined suggest this system to be one of the longer fossil-rich cave sedimentary sequences in NW Europe. Fluid inclusion isotope analysis, performed on the same material indicates that many samples are well preserved, and the
410 measured isotope values inform us on the isotope composition of past rainfall for the Scladina site. A sub-set of fluid inclusion isotope data trend away from the GMWL, which we postulate to be potentially related to diagenetic weakening of the speleothem calcite fabric. All data combined serve to remind us of the importance of careful sample selection in cave settings where burial in siliciclastic sediments has led to diagenetic overprints on speleothem calcite.

Table 2

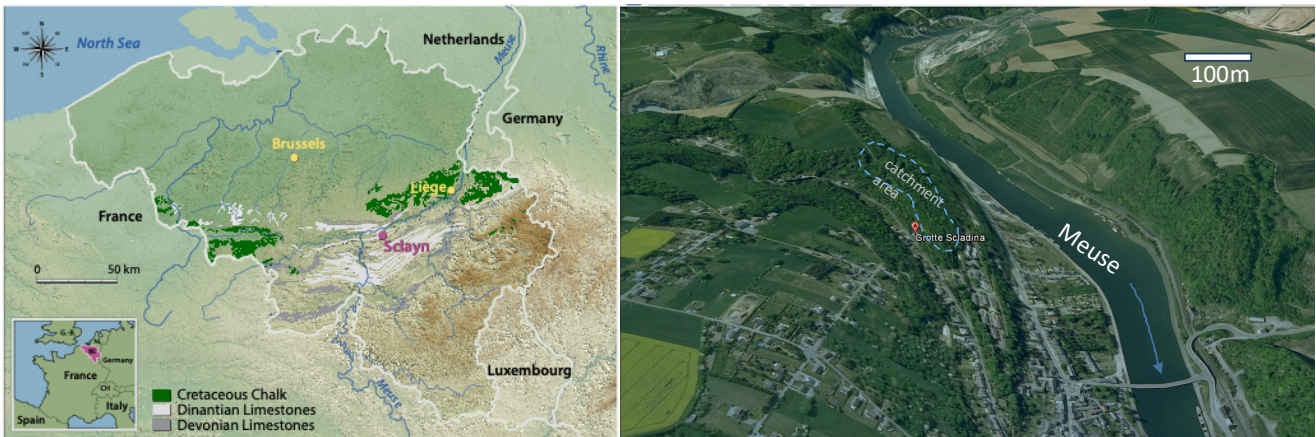
Sample	DFI [mm]	Lab	^{232}Th [ng/g]	Uncertainty	^{238}U [ng/g]	Uncertainty	$(^{234}\text{U}/^{238}\text{U})$	Uncertainty	$(^{230}\text{Th}/^{232}\text{Th})$	Uncertainty	Uncorrected Age [ka BP]	Corrected Age [ka BP]	Uncertainty [ka]
201041	22	Melbourne	0.427	0.038	0.173	0.013	1.0417	0.0036	0.00765	0.0055	9.72	0.82	0.057
201041	102	Melbourne	0.238	0.023	0.209	0.016	1.0414	0.0029	0.0096	0.0060	27.2	2.2	0.740
201041	152	Melbourne	0.332	0.032	0.211	0.016	1.0414	0.0037	0.01127	0.0091	22.4	2.3	0.943
201041	256	Melbourne	0.240	0.025	0.190	0.014	1.0516	0.0030	0.01521	0.00445	37.8	2.2	1.122
201041	330	Melbourne	0.223	0.18	0.220	0.017	1.0542	0.0031	0.02410	0.0073	7.47	0.77	1.080
201041	418	Melbourne	0.782	0.069	0.214	0.016	1.0512	0.0038	0.02793	0.0013	25.2	1.4	3.02
201042	80	Melbourne	2.18	0.19	0.211	0.016	1.0422	0.0032	0.01310	0.00665	3.99	0.24	1.316
201042	170	Melbourne	0.372	0.076	0.212	0.016	1.0480	0.0037	0.01536	0.00088	11.71	0.81	1.546
201042	415	Melbourne	2.15	0.18	0.223	0.017	1.0476	0.0037	0.02399	0.00096	9.74	0.40	3.10
201042	520	Melbourne	17.3	1.5	0.187	0.014	1.0513	0.0090	0.0669	0.0044	2.27	0.17	7.11
201245	0	Melbourne	1.26	0.10	0.196	0.015	1.0495	0.0039	0.03646	0.00049	17.84	0.32	3.788
201245	316	Melbourne	1.88	0.15	0.187	0.014	1.0400	0.0034	0.06576	0.00059	20.53	0.68	7.053
2014#206	740	Mainz IGU	1.2056	0.0076	0.1911	0.0011	1.0358	0.0005	0.08226	0.00037	39.86	0.19	8.964
2014#206	20	Xi'an	36.61	0.74	0.25821	0.0074	1.0442	0.0026	0.4608	0.0018	9.86	0.20	58.25
2014#206	40	Xi'an	11.91	0.24	0.21763	0.00031	1.0464	0.0019	0.5429	0.0013	30.33	0.61	54.84
2014#206	75	Xi'an	6.67	0.13	0.29772	0.00057	1.0895	0.0018	0.5435	0.0014	73.8	1.5	74.01
2014#206	85	Xi'an	8.91	0.18	0.23302	0.00037	1.0737	0.0017	0.5619	0.0012	44.93	0.50	79.86
201044	25	Melbourne	8.09	0.65	0.237	0.018	1.0769	0.0041	0.7199	0.00688	66.2	1.1	118.0
201044	97	Melbourne	0.333	0.075	0.254	0.019	1.0559	0.0047	0.7511	0.0066	704	17	116.1
201044	150	Melbourne	3.15	0.26	0.326	0.025	1.1301	0.0044	0.7586	0.0077	246.5	4.5	117.5
201242	40	Melbourne	0.298	0.025	0.191	0.014	1.0741	0.0030	0.7117	0.0030	1433	17	116.2
201242	225	Melbourne	0.375	0.030	0.180	0.014	1.0741	0.0030	0.7179	0.0039	1228	0.98	118.5
201242	310	Melbourne	7.81	0.64	0.198	0.015	1.0597	0.0021	0.7124	0.0037	56.58	0.59	119.70
201242	410	Melbourne	0.590	0.050	0.186	0.014	1.0669	0.0028	0.7165	0.0047	707	11	120.6
201066	2	Mainz IGU	11.66	0.12	0.2160	0.0014	1.0604	0.0016	0.7715	0.0044	40.84	0.42	122.3
201066	84	Mainz IGU	2.282	0.024	0.2332	0.0016	1.0709	0.0016	0.7222	0.0036	225.6	1.1	119.8
201066	172	Mainz IGU	3.308	0.033	0.1810	0.0012	1.0656	0.0020	0.7199	0.0038	120.4	1.1	120.6
201066	244	Mainz IGU	7.331	0.078	0.1895	0.0012	1.0768	0.0017	0.7279	0.0035	53.85	0.49	120.4
201066	35	Mainz IGU	4.237	0.030	0.2250	0.0016	1.0915	0.00042	0.8087	0.0029	148.79	0.67	142.7
201066	48	Melbourne	11.35	0.92	0.256	0.019	1.0736	0.0034	0.8024	0.0083	61.02	17.2	4.6
201066	70	Mainz IGU	1.2052	0.0085	0.2877	0.0018	1.07447	0.00033	0.8694	0.0033	634.3	3.1	174.0
2014#618-2-SV112	3	Xi'an	3.289	0.066	0.2567	0.00029	1.0492	0.0012	0.8857	0.0013	212.0	4.3	196.5
2014#618-2-SV112	80	Mainz IGU	0.3935	0.0055	0.2337	0.0015	1.0549	0.0013	0.8934	0.0013	87.3	1.8	196.7
2014#618-3	80	Mainz IGU	1.2052	0.0085	0.2877	0.0018	1.07447	0.00033	0.8694	0.0033	634.3	3.1	174.0
201244	20	Melbourne	0.703	0.059	0.184	0.014	1.1094	0.0026	1.0734	0.0046	883	11	303.7
201244	48	Mainz IGU	1.156	0.012	0.1475	0.0010	1.0669	0.0020	1.0679	0.0039	416.6	4.1	300.4
201244	48	Melbourne	5.73	0.47	0.147	0.011	1.0443	0.0023	1.0728	0.0052	66.30	0.95	311.1
201244	84	Melbourne	9.49	0.81	0.192	0.014	1.074	0.0029	1.0789	0.0052	67.8	1.0	302.5
201244	15	Melbourne	1.057	0.013	0.276	0.021	1.0849	0.0024	1.0649	0.0057	6040	83	429
201244	20	Melbourne	0.852	0.0018	0.2941	0.0020	1.0838	0.0023	1.1026	0.0100	11630	260	477
201244	35	Melbourne	0.213	0.018	0.240	0.018	1.0881	0.0034	1.0988	0.0049	3895	59	431
201244	50	Melbourne	0.141	0.012	0.381	0.018	1.0907	0.0030	1.1031	0.0055	9379	100	430
201244	50	Mainz IGU	0.0722	0.0016	0.5491	0.0016	1.0982	0.0027	1.092	0.011	23370	580	363
201244	10	Xi'an	0.903	0.012	0.3358	0.0039	1.0822	0.0012	1.1001	0.0016	1894	38	475
201244	60	Xi'an	1.1411	0.0029	0.29206	0.00032	1.0876	0.0012	1.1150	0.0017	7060	40	536
201244	60	Xi'an	1.1411	0.0029	0.29206	0.00032	1.0876	0.0012	1.1150	0.0017	7060	40	536

Table 1: Results of the $^{230}\text{Th}/\text{U}$ -dating of the Sladina samples. The ages are given in ka before 1950

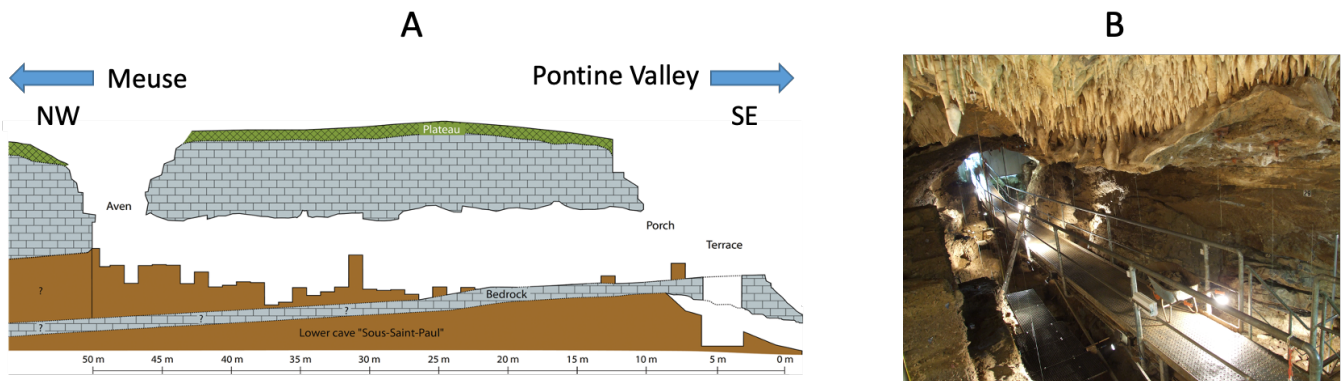
Sample	DFT cm	$\delta^{13}\text{C}_{\text{cc}}$ VPDB	$\delta^{18}\text{O}_{\text{cc}}$ VPDB	CaCO ₃ weight g	yield μl	rel yield μl/g	$\delta^{18}\text{O}_{\text{fi}}$ VSMOW	$\delta^2\text{H}_{\text{fi}}$ VSMOW	calculated T °C
2012#5	29	-	-	0.50	0.27	0.54	-4.97	-43.08	-
2012#5	20	-8.8	-4.4	0.60	0.25	0.42	-6.05	-46.66	11.1
2012#5	2	-6.7	-3.9	0.40	0.26	0.65	-5.94	-44.69	8.8
2012#5	2	-7.0	-4.2	0.40	0.20	0.50	-6.95	-47.01	5.3
2012#5	2	-6.9	-4.2	0.30	0.18	0.60	-6.04	-45.49	9.7
2012#5	25	-6.8	-3.8	0.40	0.09	0.23	-6.86	-46.42	4.1
2012#5	10	-7.8	-4.5	0.40	0.18	0.45	-4.54	-42.76	19.4
2012#5	41	-8.5	-4.6	0.50	0.40	0.80	-6.21	-43.83	10.9
2012#5	10	-7.8	-4.6	0.40	0.21	0.53	-4.88	-44.44	17.9
2012#5	5	-8.1	-4.2	0.50	0.30	0.60	-5.21	-43.12	14.0
2012#5	29	-8.5	-4.6	0.60	0.48	0.80	-5.21	-43.89	16.0
2012#5	45	-7.5	-4.2	0.46	0.21	0.46	-2.89	-39.84	26.4
2012#5	50	-8.6	-4.8	0.70	0.28	0.40	-6.41	-44.29	11.3
2012#5	45.5	-8.4	-4.6	0.72	0.20	0.28	-5.29	-41.6	15.6
2012#5	60	-7.8	-4.8	0.38	0.33	0.87	-7.04	-46.86	7.9
2012#5	70	-8.4	-4.9	0.39	0.07	0.18	-4.73	-41.35	20.5
2012#5	60	-7.6	-4.6	0.40	0.41	1.03	-6.96	-46.51	7.4
2012#5	70	-8.8	-4.9	0.57	0.14	0.25	-3.907	-40.36	25.0
2010#2	50	-8.0	-4.4	0.68	0.05	0.07	-	-	-
2010#2	7	-10.0	-5.1	0.90	0.33	0.37	-6.11	-42.12	13.9
2010#1	37	-10.3	-5.5	0.70	0.34	-	-6.62	-47.13	13.5
2010#2	24	-10.0	-5.3	0.81	0.29	0.36	-6.96	-44.68	10.6
2010#1	11	-8.6	-4.6	0.56	0.05	0.09	-	-	-
2010#1	27	-10.9	-5.2	0.76	0.28	0.37	-7	-44.38	10.1
2012#4	2	-9.5	-5.0	0.81	1.01	1.25	-7.67	-53.62	5.8
2012#4	8	-8.7	-4.9	0.46	1.02	2.22	-7.56	-53.8	5.8
2012#4	2	-9.7	-5.0	0.27	0.51	1.89	-7.6	-54.39	6.3
2012#4	8	-9.0	-4.9	0.33	0.54	1.64	-7.98	-55.49	3.9
2012#1	21	-7.0	-3.4	0.45	0.03	0.07	-	-	-
2012#1	2	-9.4	-4.6	0.87	0.29	0.33	-6.89	-46.43	7.8
2012#1	10	-8.6	-4.3	0.95	0.44	0.46	-6.68	-44	7.1
2012#1	21	-7.6	-3.6	0.98	0.20	0.20	-4.74	-41.09	13.3
2012#2	38	-7.4	-3.9	0.90	0.43	0.48	-6.08	-43.49	8.4
2012#2	19	-5.2	-3.2	0.89	0.31	0.35	-5.12	-41.9	9.3
2012#2	4	-9.0	-4.2	0.75	0.40	0.53	-6.78	-46.92	6.4
2012#2	31	-8.1	-4.2	0.78	0.41	0.53	-6.53	-44.01	7.4
2010#14	30	-8.6	-4.5	0.79	0.18	0.23	-4.25	-41.21	20.5
2010#14	19	-8.4	-4.7	0.88	0.15	0.17	-5.91	-44.44	13.1
2010#14 some visible diagenesis	22	-5.3	-3.2	0.74	0.02	0.03	-	-	-
2010#6	10	-8.8	-4.7	0.88	0.41	0.47	-6.17	-44.07	11.7
2010#6	4	-8.2	-4.1	0.80	0.22	0.28	-1.27	-37.77	35.6
2010#6	13	-7.9	-3.9	0.84	0.17	0.20	-0.65	-36.58	37.5
2010#6	6	-8.0	-4.1	0.93	0.51	0.55	-6.35	-46.06	7.6
2010#6	4	-8.1	-4.1	0.80	0.05	0.06	-	-	-
2014#618-3 base	10	-7.9	-4.1	0.80	0.44	0.55	-6.25	-44.52	8.3
2014#618-3 Middle	5	-7.0	-4.3	0.79	0.56	0.71	-6.47	-44.61	8.1
2014#618-3 side some visible diagenesis	-	-5.41	-3.62	0.68	0.02	0.03	-	-	-
2014#618-3 top side significant visible diagenesis	-	-	-	1.10	failed	-	-	-	-
2014#206 base of stal	90	-7.01	-4.45	0.50	0.93	1.86	-6.75	-49.29	7.6
2014#206	24	-7.97	-4.88	0.50	0.64	1.28	-5.45	-47.48	16.3
drip water sample Sladina Cave							-6.48	-42.40	

Table 2: Stable isotope data of Sladina Cave fluid inclusion water samples, and one drip water sample (bottom). Also indicated are the stable isotope values of the host calcite of the fluid inclusion samples, and the calculated temperatures from the paired fluid

425 inclusion and host calcite oxygen isotope ratios. This calculation is based on the (Tremaine et al., 2011) equation. DFT = distance from top.



430 Fig. 1: Left: Map of Belgium with the town Sclayn indicated, where Scladina Cave is situated. Right: Aerial view of Scladina Cave, accessible from the Pontine valley, (© Google Earth 2020). Indicated in blue is our rough approximation of the catchment area of 430 dripwater in the cave.



435 Fig. 2: A) Schematic cross section of Scladina Cave and the underlying Sous Saint Paul Cave (Bonjean et al., 2014). The entrance at the SE side is nowadays closed by a door. B) scaffolding and walkways installed in the cave, and positioning lines that mark the archeological excavation grid. The irregular cave sediment depth (brown) represents the ongoing archeological excavation activity. The lower Sous-Saint-Paul cave is in connection with the upper gallery through vertical pits that are mostly filled with sediments. Only the connection in the entrance zone is visible in the figure.

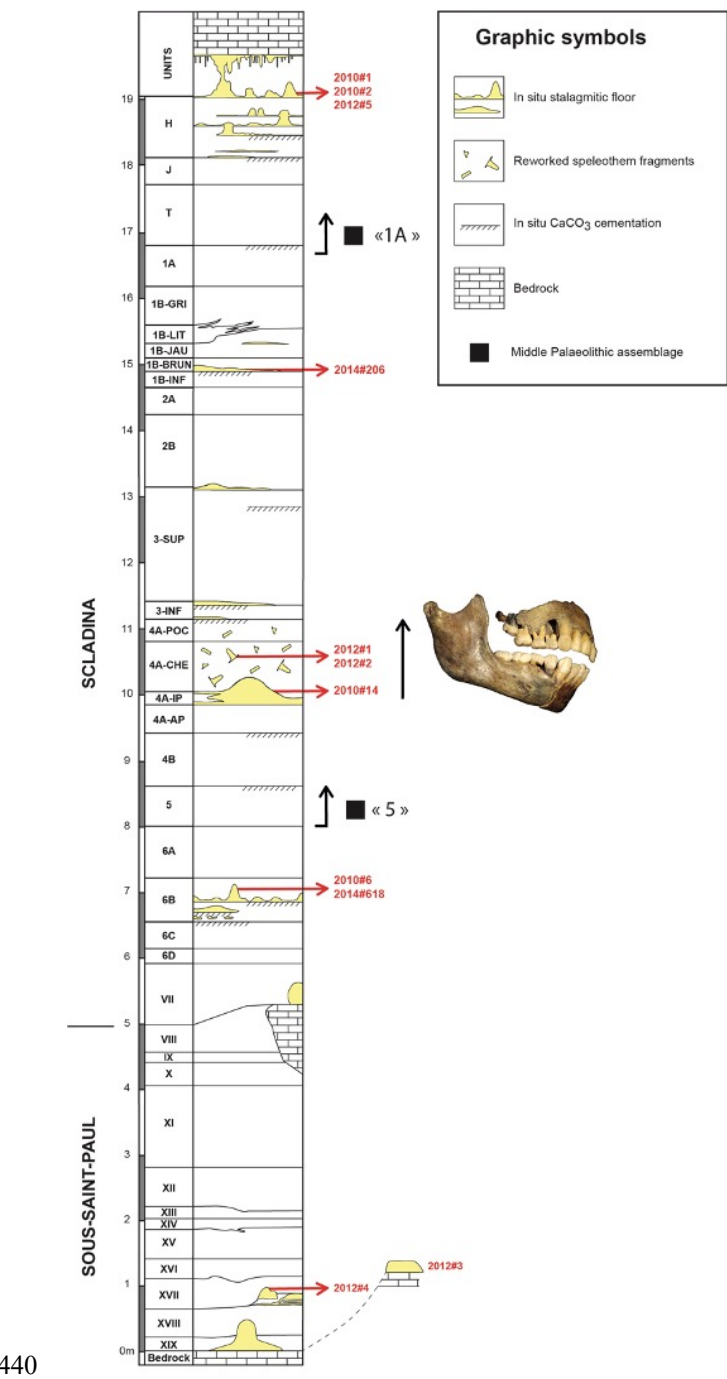
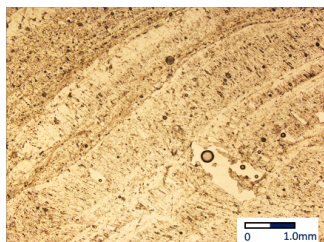
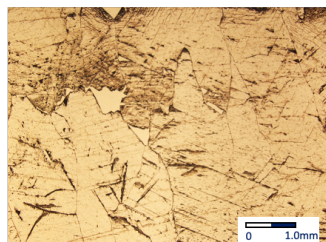


Fig. 3: Schematic stratigraphic column of the combined Scladina and Sous-Saint-Paul cave sedimentary sequence. Speleothem occurrences are indicated in yellow coloring. Vertical scale bar is in meters. The position of the samples that were dated in this study is indicated by the red arrows. Photograph indicates the position of the Neandertal mandible and teeth found in unit 4A.

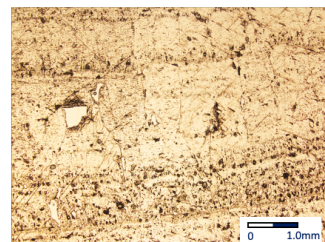
2012#2



2012#3



2012#4



2012#6

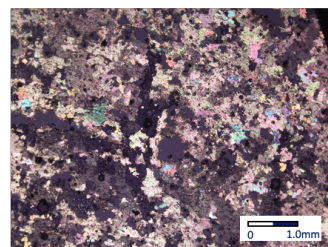
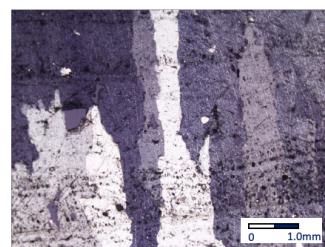
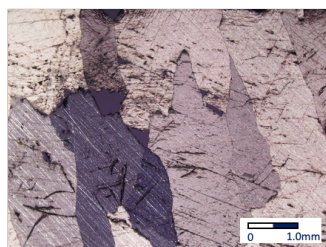
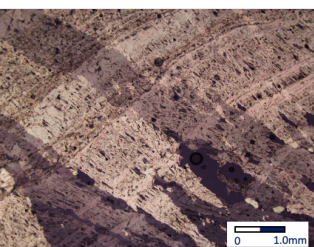
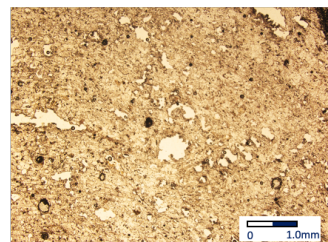
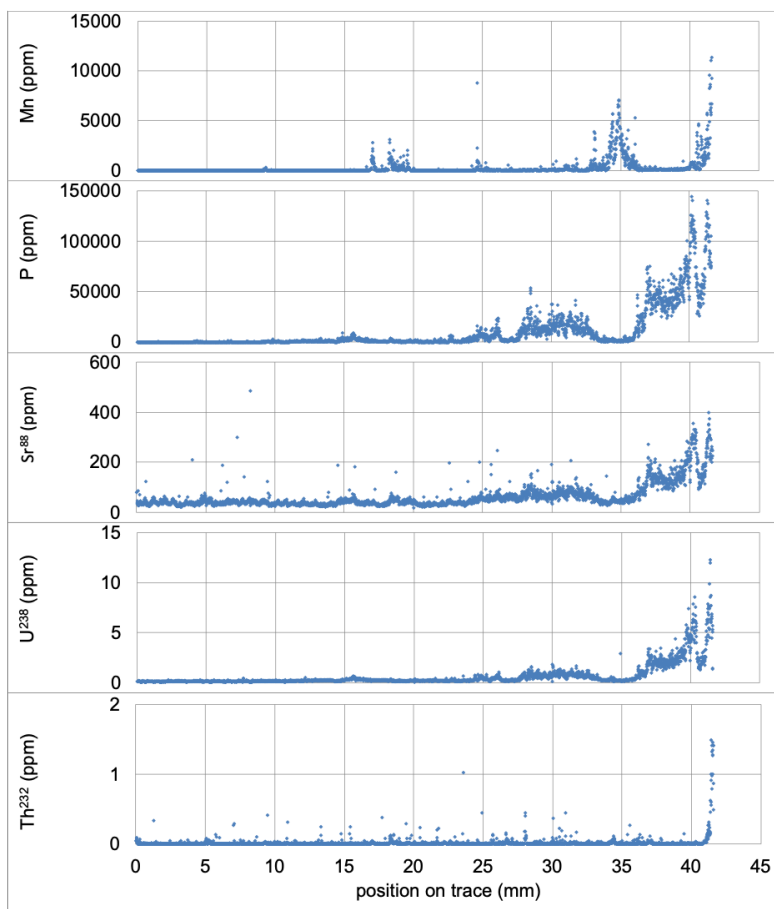
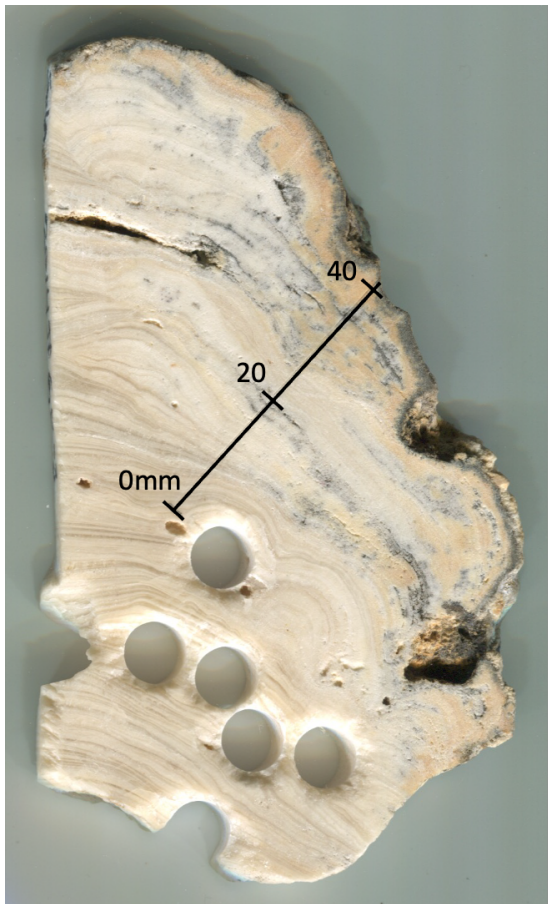


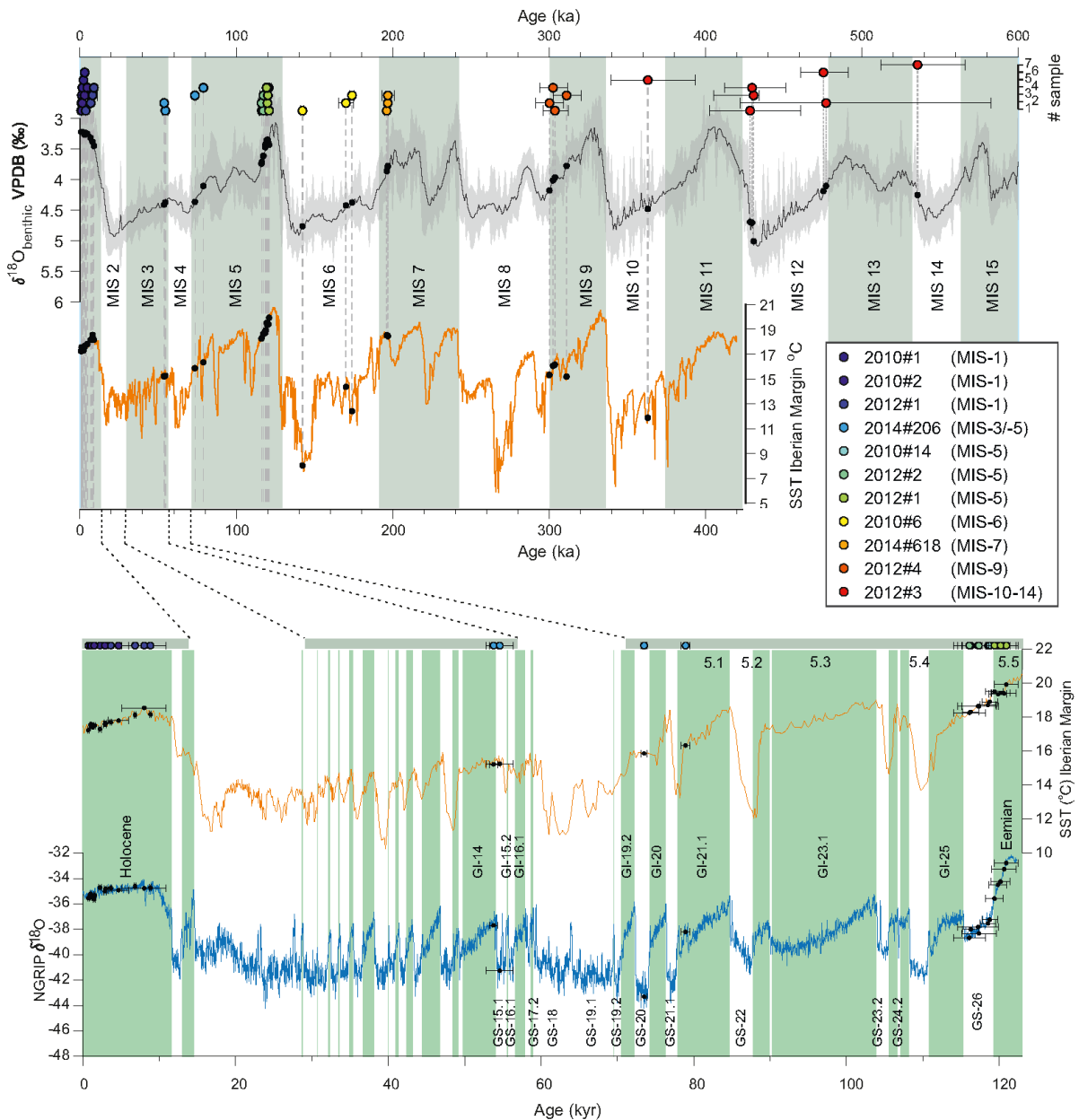
Fig. 4: Some representative thin section images of the speleothem material studied. The top row are plain light (PL) images, with the growth direction generally upward. The bottom row are the same pictures, in cross polarized light (CPL). Specimens 2012#2 and 2012#4 show micro-scale growth banding of speleothem calcite in PL and cross-cutting columnar crystallographic fabric visible in CPL, which we interpret to reflect well-preserved speleothem calcite. Fluid inclusions in these images are shown as small black dots that generally line up along the growth bands. The images of specimen 2012#3 show no growth banding, relatively coarse crystals that are elongated in the growth direction, and a conspicuous scarcity of fluid inclusions. The images of specimen 2012#6 show a lack of growth banding and very small equidimensional crystals which we interpret to indicate diagenetic alteration of speleothem calcite. That specimen was discarded, and has not further been analysed in this study.

450

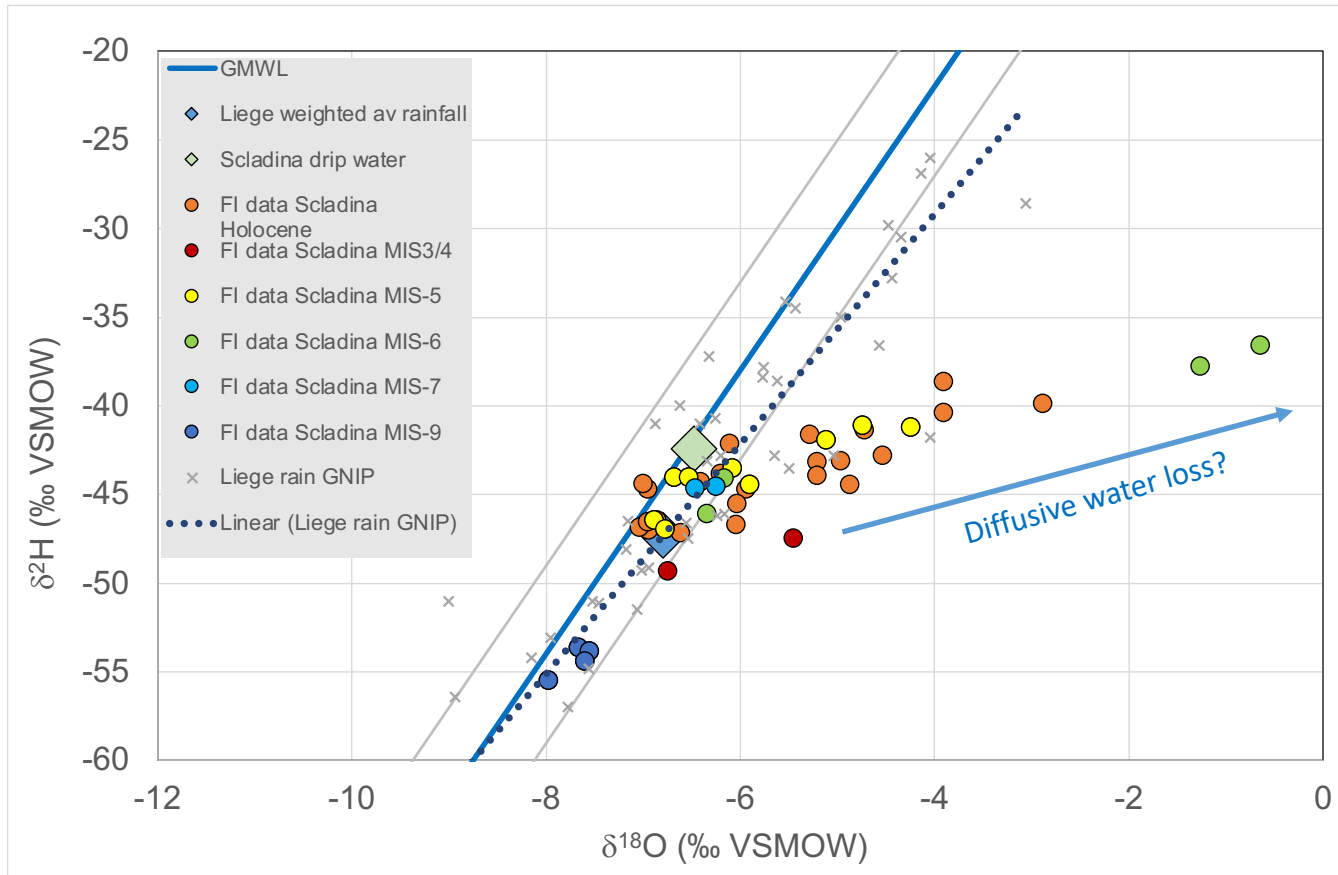
455



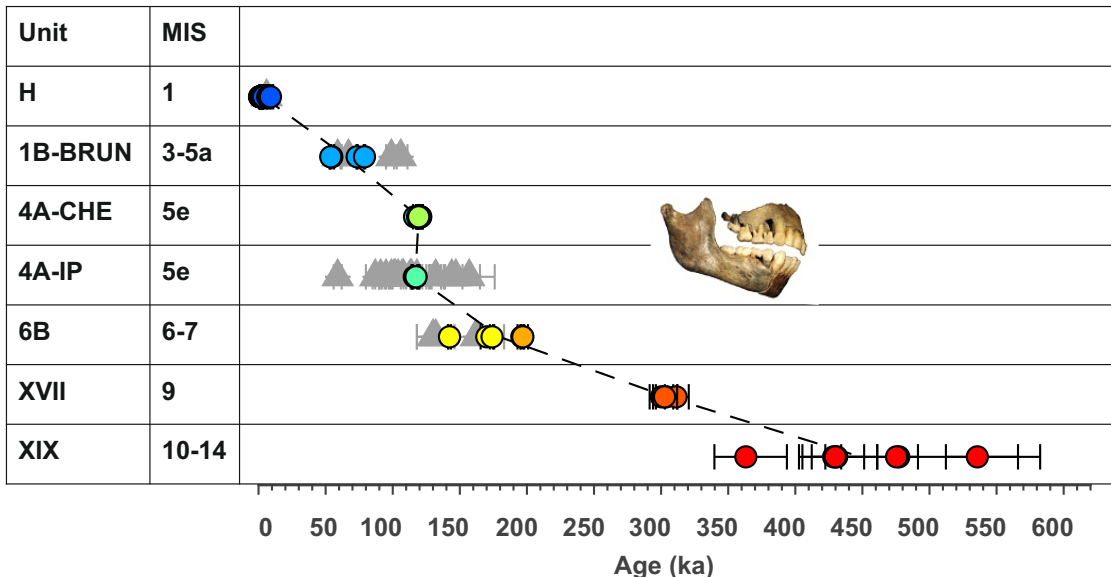
460 Fig. 5: Stalagmite sample 2014#618 shows clear discoloration towards the right side of the stalagmite that was exposed to the
 465 sediment in which it was buried. Laser ablation trace element analysis along the 42 mm long transect shown on the picture
 demonstrates that Manganese is associated with the blackish layers that occur in the exterior portions of the stalagmite. It is further
 clear that significant enrichment of U and Th occurs at the surface of the stalagmite that has been in contact with the sediment
 in which it was covered. Uranium declines gradually from the outer surface towards the center of the stalagmite. Sr shows a similar
 pattern to U. The Th content of the entire trace can be considered very low, with the exception of the increased Th concentration on
 the outer surface. Circular holes in the basal part of the sample are samples taken for earlier investigations, unrelated to the present
 study.



470 Fig. 6: The U-Th ages of the individual speleothems that were obtained in this study are plotted as coloured dots with their 2σ -
 uncertainty limits, and are projected onto global and regional climate proxy records. The global benthic $\delta^{18}\text{O}$ probabilistic stack
 (Ahn et al., 2017) with the mean and 95% confidence interval given as a black solid line and grey areas, respectively. This global
 benthic $\delta^{18}\text{O}$ stack provides the glacial-interglacial variability, whereby the glacial and interglacial (grey bars) Marine Isotope Stages
 475 are defined by Lisicki and Raymo (2005). The orange line indicates the UK'37 sea surface temperature (SST) record from marine
 sediment core MD01-2443 off the Iberian Margin (Martrat et al., 2007). The high-resolution $\delta^{18}\text{O}$ record of the North Greenland
 Ice Core Project (NGRIP) site is plotted as a blue line together with the Greenland stadials (GS) and interstadials (GI: green bars)
 (Rasmussen et al., 2014; Seierstad et al., 2014).



480 Fig. 7: fluid inclusion isotope data of Scladina speleothems shown as round plot symbols. GNIP rainfall isotope data for Liege in the time period between 1966 and 1970 are indicated as grey crosses. The GMWL is shown as a blue line, the local (Liege) MWL as the dotted blue line. Parallel grey lines indicate the GMWL+5 to GMWL-5 envelope around the GMWL. Annually averaged rainwater isotope value and the drip water isotope composition in the cave is shown as diamonds.



485

Fig. 8: Schematic overview of the U-Th ages of the present study (color scheme the same as Fig 6), compared with, in grey, earlier U-Th ages, as summarized in Bonjean (1998). Unit numbers are conform the stratigraphic column in Fig. 3. Please note that units without U-Th ages are not shown. Dashed line connects the median values of the ages from the current study.

490

Appendix A



Fig. A1: Overview of slabs cut from the stalagmite specimens studied. The drill-holes visible on many of the slabs were made for earlier student project analyses. Precise locations of samples in the present study can be retrieved from Table 1

500

Appendix B

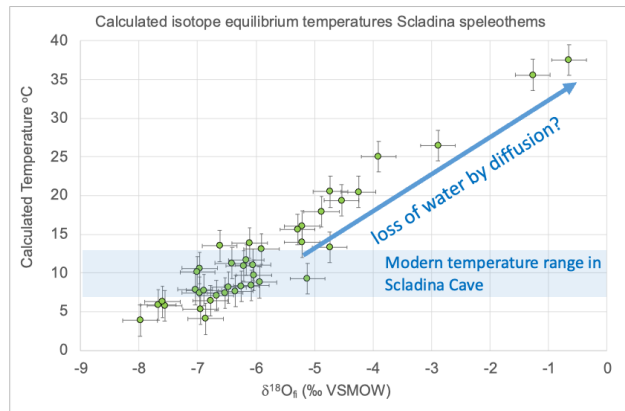
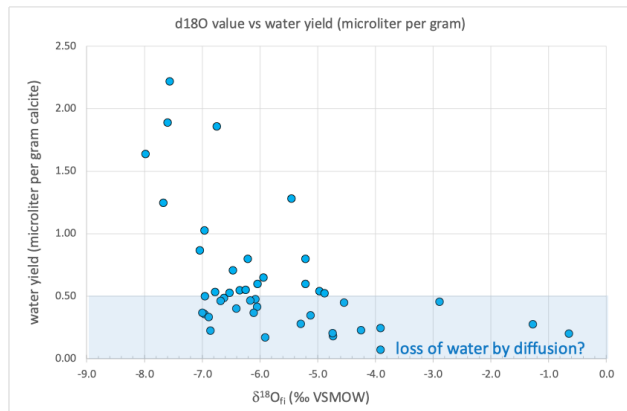
A**B**

Fig. B1 A) Isotope equilibrium temperatures calculated from paired oxygen isotope values of fluid inclusions and their host calcite. The blue shaded box spans the modern seasonal temperature variation measured in the cave. Higher $\delta^{18}\text{O}_{\text{fi}}$ values lead to unrealistically high temperatures, suggesting that the process that leads the fluid inclusion values away from the GMWL sends the fluid inclusions and their host calcite out of isotopic equilibrium. B) Cross plot showing that lower water yield samples tend to have higher $\delta^{18}\text{O}_{\text{fi}}$ values. Blue zone indicates samples with lower than 0.5 microliter per gram extraction yields which we postulate to be the samples that may have lost water through diffusion, leading the remaining water to be isotopically fractionated towards higher $\delta^{18}\text{O}_{\text{fi}}$ values.

505

510

Data availability:

Laser ablation trace element data used in this publication is available at: <https://doi.org/10.17617/3.UKDF4T>

515

Author contribution

H.B.V coordinated the project in which M.A.P.v.N., J.R. M.v.d.D, and D.B. performed lab work and analyses. Samples were collected and placed in the stratigraphical context by D.B., S.P. K.d.M and G.A. J.H., D.S., M.W. S.V., H.C and X.J. provided 520 U-Th analyses. J.v.d.L., D.B. and S.P. provided material for figures. H.B.V. prepared the manuscript with contributions from all co-authors.

Competing interests

525 The authors declare that they have no conflict of interest

Acknowledgements

This study is the cumulative result of many years of research effort of students at Vrije Universiteit Amsterdam, and later at 530 the Max Planck Institut für Chemie, and the Johannes Gutenberg Universität, Mainz. This project would not even have started if it were not for the enthusiastic support by Dick Kroon, at that point in time Professor at the Earth Sciences Department at Vrije Universiteit Amsterdam. With his broad interest in new paleoceanographical and paleoclimatological proxy systems and techniques Dick supported and motivated HV to initiate a line of speleothem research that has been developing until today. Special acknowledgement goes to Laura García Soler, one of the students who contributed to this study. We have unfortunately 535 not been able to reach her to offer co-authorship on this ms.

References

540 Ahn, S., Khider, D., Lisiecki, L. E., and Lawrence, C. E.: A probabilistic Pliocene–Pleistocene stack of benthic $\delta^{18}\text{O}$ using a profile hidden Markov model, *Dynamics and Statistics of the Climate System*, 2, 10.1093/climsys/dzx002, 2017.

Audra, P., Heresau, V., Barriquand, L., El Kadiri Boutchich, M., Jaillet, S., Pons-Branchu, E., Bosak, P., Cheng, H., Edwards, R. L., and Renda, M.: Bat guano minerals and mineralization processes in Chameau Cave, Eastern Morocco, *Int J Speleol*, 50, 91-109, 10.5038/1827-806x.50.1.2374, 2021.

545 Bajo, P., Hellstrom, J., Frisia, S., Drysdale, R., Black, J., Woodhead, J., Borsato, A., Zanchetta, G., Wallace, M. W., Regattieri, E., and Haese, R.: "Cryptic" diagenesis and its implications for speleothem geochronologies, *Quaternary Science Reviews*, 148, 17-28, 10.1016/j.quascirev.2016.06.020, 2016.

Bard, E., Antonioli, F., and Silenzi, S.: Sea-level during the penultimate interglacial period based on a submerged stalagmite from Argentarola Cave (Italy), *Earth and Planetary Science Letters*, 196, 135-146, 10.1016/s0012-821x(01)00600-8, 2002.

550 Bastin, B.: Analyse pollinique des sédiments détritiques, des coprolithes et des concrétions du site préhistorique de la grotte Scladina (Province de Namur, Belgique), in, 59-77, 1992.

Bocherens, H.: Diet and ecology of the Scladina I-4A Neandertal child: insights from stable isotopes, in: *The Scladina I-4A juvenile Neandertal*, edited by: Toussaint, M., and Bonjean, D., *Études et recherches archéologiques de l'Université de Liège*, 134, ERAUL, Liège, 351-362, 2014.

555 Bocherens, H., Billiou, D., Patou-Mathis, M., Bonjean, D., Otte, M., and Mariotti, A.: Paleobiological implications of the isotopic signatures (C-13, N-15) of fossil mammal collagen in Scladina cave (Sclayn, Belgium), *Quaternary Res*, 48, 370-380, DOI 10.1006/qres.1997.1927, 1997.

Bonjean, D.: Chronologie à la grotte Scladina, in: *Recherches aux grottes de Sclayn*, vol 2, l'Archéologie, edited by: Otte, M., Patou-Mathis, M., and Bonjean, D., *Études et recherches archéologiques de l'Université de Liège*, 134, ERAUL, Liège, 45-57, 1998.

560 Bonjean, D., Toussaint, M., and Otte, M.: Scladina (Sclayn, Belgique) : l'homme de néandertal retrouvé!, *Notae Praehistoricae*, 16, 37-46, 1996.

Bonjean, D., Abrams, G., Di Modica, K., Otte, M., Pirson, S., and Toussaint, M.: Scladina Cave: Archeological context and history of the discoveries, in: *The Scladina I-4A juvenile Neandertal*, edited by: Toussaint, M., and Bonjean, D., *Études et recherches archéologiques de l'Université de Liège*, 134, ERAUL, Liège, 31-48, 2014.

565 Cheng, H., Edwards, R. L., Shen, C. C., Polyak, V. J., Asmerom, Y., Woodhead, J., Hellstrom, J., Wang, Y. J., Kong, X. G., Spötl, C., Wang, X. F., and Alexander, E. C.: Improvements in Th-230 dating, Th-230 and U-234 half-life values, and U-Th isotopic measurements by multi-collector inductively coupled plasma mass spectrometry, *Earth and Planetary Science Letters*, 371, 82-91, 10.1016/j.epsl.2013.04.006, 2013.

570 Cheng, H., Zhang, H., Spötl, C., Baker, J., Sinha, A., Li, H., Bartolomé, M., Moreno, A., Kathayat, G., Zhao, J., Dong, X., Li, Y., Ning, Y., Jia, X., Zong, B., Ait Brahim, Y., Pérez-Mejías, C., Cai, Y., Novello, V. F., Cruz, F. W., Severinghaus, J. P., An, Z., and Edwards, R. L.: Timing and structure of the Younger Dryas event and its underlying climate dynamics, *Proceedings of the National Academy of Sciences*, 117, 23408-23417, 10.1073/pnas.2007869117, 2020.

Cordy, J.-M. and Bastin, B.: Synthèse des études paléontologiques réalisées dans les dépôts de la grotte Scladina (Sclayn, Province de de Namur), in, 153-156, 1992.

575 de Graaf, S., Vonhof, H. B., Weissbach, T., Wassenburg, J. A., Levy, E. J., Kluge, T., and Haug, G. H.: A comparison of isotope ratio mass spectrometry and cavity ring-down spectroscopy techniques for isotope analysis of fluid inclusion water, *Rapid Communications in Mass Spectrometry*, 34, ARTN e8837 10.1002/rcm.8837, 2020.

Dennis, P. F., Rowe, P. J., and Atkinson, T. C.: The recovery and isotopic measurement of water from fluid inclusions in speleothems, *Geochimica Et Cosmochimica Acta*, 65, 871-884, Doi 10.1016/S0016-7037(00)00576-7, 2001.

580 Fernandez, A., Løland, M. H., Maccali, J., Krüger, Y., Vonhof, H. B., Sodemann, H., and Meckler, A. N.: Characterization and Correction of Evaporative Artifacts in Speleothem Fluid Inclusion Isotope Analyses as Applied to a Stalagmite From Borneo, *Geochemistry, Geophysics, Geosystems*, 24, e2023GC010857, <https://doi.org/10.1029/2023GC010857>, 2023.

Frisia, S.: Microstratigraphic logging of calcite fabrics in speleothems as tool for palaeoclimate studies, *Int J Speleol*, 44, 1-16, 10.5038/1827-806x.44.1.1, 2015.

585 Frisia, S., Borsato, A., Fairchild, I. J., and McDermott, F.: Calcite fabrics, growth mechanisms, and environments of formation in speleothems from the Italian Alps and southwestern Ireland, *J Sediment Res*, 70, 1183-1196, Doi 10.1306/022900701183, 2000.

Gewelt, M., Schwarcz, H. P., and Szabo, B. J.: Datations 230Th/234U et 14C de concrétions stalagmitiques de la grotte Scladina. Volume 1 : Le contexte, in: *Recherches aux grottes de Sclayn*, , edited by: Otte, M., Etudes et recherches Archeologiques de l'Université de Liège, 27, Universite de Liège, Liège, 159-172, 1992.

Hellstrom, J.: Rapid and accurate U/Th dating using parallel ion-counting multi-collector ICP-MS, *J Anal Atom Spectrom*, 18, 10.1039/b308781f, 2003.

Huxtable, J. and Aitken, M. J.: Thermoluminescence dating of burned flint and stalagmitic calcite from grottes de Sclayn (Namur). in: *Recherches aux grottes de Sclayn*, Volume 1, Le contexte, edited by: Otte, M., Etudes et recherches Archeologiques de l'Université de Liège, 27, Universite de Liège, Liège, 175-178, 1992.

IAEA/WMO: Global Network of Isotopes in Precipitation. The GNIP Database. Accessible at: <https://nucleus.iaea.org/wiser>, 2023.

600 Jochum, K. P., Scholz, D., Stoll, B., Weis, U., Wilson, S. A., Yang, Q., Schwalb, A., Börner, N., Jacob, D. E., and Andreae, M. O.: Accurate trace element analysis of speleothems and biogenic calcium carbonates by LA-ICP-MS, Chemical Geology, 318-319, 31-44, 10.1016/j.chemgeo.2012.05.009, 2012.

KMI: Klimaatstatistieken van de Belgische gemeenten. Accessible at: <https://www.meteo.be/nl/klimaat/klimaat-van-belgie/klimaat-in-uw-gemeente>, 2024.

605 Kroon, D., Alexander, I. T., Little, M. G., Lourens, L. J., Matthewson, A., Robertson, A. H. F., and Sakamoto, T.: Stable isotope record and age model for sapropel stratigraphy of ODP Site 160-967, 10.1594/PANGAEA.790405, 1998.

Lechleitner, F. A., Amirnezhad-Mozhdehi, S., Columbu, A., Comas-Bru, L., Labuhn, I., Pérez-Mejías, C., and Rehfeld, K.: The Potential of Speleothems from Western Europe as Recorders of Regional Climate: A Critical Assessment of the SISAL Database, Quaternary, 1, 10.3390/quat1030030, 2018.

610 Lisiecki, L. E. and Raymo, M. E.: A Pliocene-Pleistocene stack of 57 globally distributed benthic $\delta^{18}\text{O}$ records, Paleoceanography, 20, 10.1029/2004pa001071, 2005.

Martrat, B., Grimalt, J. O., Shackleton, N. J., de Abreu, L., Hutterli, M. A., and Stocker, T. F.: Four Climate Cycles of Recurring Deep and Surface Water Destabilizations on the Iberian Margin, Science, 317, 502-507, 10.1126/science.1139994, 2007.

615 Obert, J. C., Scholz, D., Felis, T., Brocas, W. M., Jochum, K. P., and Andreae, M. O.: 230Th/U dating of Last Interglacial brain corals from Bonaire (southern Caribbean) using bulk and theca wall material, Geochimica et Cosmochimica Acta, 178, 20-40, 10.1016/j.gca.2016.01.011, 2016.

Orlando, L., Darlu, P., Toussaint, M., Bonjean, D., Otte, M., and Hanni, C.: Revisiting Neandertal diversity with a 100,000 year old mtDNA sequence, Current Biology, 16, R400-R402, DOI 10.1016/j.cub.2006.05.019, 2006.

Otte, M. (Ed.) Recherches aux grottes de Sclayn. Volume 1 : Le contexte. , Etudes et Recherches archéologiques de l'Université de Liège, 1, l'Université de Liège, Liege, 178 pp., 1992.

620 Otte, M., Toussaint, M., and Bonjean, D.: Découverte de restes humains immatures dans les niveaux moustériens de la grotte Scladina à Andenne (Belgique). Bulletins et Mémoires de la Société d'Anthropologie de Paris, nouvelle série, 5, 327-332, 1993.

Peral, M., Marchegiano, M., Verheyden, S., Goderis, S., Van Helden, T., Vanhaecke, F., Van Acker, T., Jia, X., Cheng, H., 625 Fiebig, J., Fourcade, T., Snoeck, C., and Claeys, P.: A new insight of the MIS 3 Dansgaard-Oeschger climate oscillations in western Europe from the study of a Belgium isotopically equilibrated speleothem, Quaternary Science Reviews, 329, 10.1016/j.quascirev.2024.108564, 2024.

Peyregne, S., Slon, V., Mafessoni, F., de Filippo, C., Hajdinjak, M., Nagel, S., Nickel, B., Essel, E., Le Cabec, A., 630 Wehrberger, K., Conard, N. J., Kind, C. J., Posth, C., Krause, J., Abrams, G., Bonjean, D., Di Modica, K., Toussaint, M., Kelso, J., Meyer, M., Paabo, S., and Prufer, K.: Nuclear DNA from two early Neandertals reveals 80,000 years of genetic continuity in Europe, Sci Adv, 5, ARTN eaaw5873 10.1126/sciadv.aaw5873, 2019.

Pirson, S.: Contribution à l'étude des dépôts d'entrée de grotte en Belgique au Pléistocène supérieur. Stratigraphie, 635 sédimentogenèse et paléoenvironnement., PhD, University of Liège and Royal Belgian Institute of Natural Sciences, 435 pp., 2007.

Pirson, S.: The stratigraphic sequence of Scladina Cave, in: The Scladina I-4A juvenile Neandertal, edited by: Toussaint, M., and Bonjean, D., Études et recherches archéologiques de l'Université de Liège, 134, ERAUL, Liège, 69 - 92, 2014.

Pirson, S., Bonjean, D., and Toussaint, M.: Stratigraphic origin of the juvenile Neandertal remains from Scladina Cave: re-evaluation and consequences for their palaeoenvironmental and chronostratigraphic contexts, in: The Scladina I-4A juvenile Neandertal, edited by: Toussaint, M., and Bonjean, D., Études et recherches archéologiques de l'Université de Liège, 134, ERAUL, Liège, 93-115, 2014a.

640 Pirson, S., Court-Picon, M., Haesaerts, P., Bonjean, D., and Damblon, F.: New data on geology, anthracology and palynology from the Scladina Cave Pleistocene sequence: preliminary results, Memoirs of the geological survey of Belgium, 55, 71-93, 2008.

Pirson, S., Court-Picon, M., Damblon, F., Balescu, S., Bonjean, D., and Haesaerts, P.: The paleoenvironmental context and chronostratigraphic framework of the Scladina Cave sedimentary sequence (units 5 to 3-sup), in: The Scladina I-4A juvenile

645 Neandertal, edited by: Toussaint, M., and Bonjean, D., *Études et recherches archéologiques de l'Université de Liège*, 134, ERAUL, Liège, 69 - 92, 2014b.

Quinif, Y.: Complex stratigraphic sequences in Belgian caves correlation with climatic changes during the Middle, the Upper Pleistocene and the Holocene, *Geol Belg*, 9, 231-244, 2006.

650 Rasmussen, S. O., Bigler, M., Blockley, S. P., Blunier, T., Buchardt, S. L., Clausen, H. B., Cvijanovic, I., Dahl-Jensen, D., Johnsen, S. J., Fischer, H., Gkinis, V., Guillevic, M., Hoek, W. Z., Lowe, J. J., Pedro, J. B., Popp, T., Seierstad, I. K., Steffensen, J. P., Svensson, A. M., Valletonga, P., Vinther, B. M., Walker, M. J. C., Wheatley, J. J., and Winstrup, M.: A stratigraphic framework for abrupt climatic changes during the Last Glacial period based on three synchronized Greenland ice-core records: refining and extending the INTIMATE event stratigraphy, *Quaternary Science Reviews*, 106, 14-28, <https://doi.org/10.1016/j.quascirev.2014.09.007>, 2014.

655 Riechelmann, D. F. C., Albert, J., Britzius, S., Krebsbach, F., Scholz, D., Schenk, F., Jochum, K. P., and Sirocko, F.: Bioproductivity and vegetation changes documented in Eifel maar lake sediments (western Germany) compared with speleothem growth indicating three warm phases during the last glacial cycle, *Quaternary International*, 673, 1-17, 10.1016/j.quaint.2023.11.001, 2023.

660 Sancho, C., Arenas, C., Vázquez-Urbez, M., Pardo, G., Lozano, M. V., Peña-Monné, J. L., Hellstrom, J., Ortiz, J. E., Osácar, M. C., Auqué, L., and Torres, T.: Climatic implications of the Quaternary fluvial tufa record in the NE Iberian Peninsula over the last 500 ka, *Quaternary Res*, 84, 398-414, 10.1016/j.yqres.2015.08.003, 2015.

665 Scholz, D. and Hoffmann, D.: 230Th/U-dating of fossil corals and speleothems, *Quaternary Science Journal*, 57, 52-76, 2008.

Scholz, D., Tolzmann, J., Hoffmann, D. L., Jochum, K. P., Spötl, C., and Riechelmann, D. F. C.: Diagenesis of speleothems and its effect on the accuracy of 230 Th/U-ages, *Chemical Geology*, 387, 74-86, 10.1016/j.chemgeo.2014.08.005, 2014.

670 Seierstad, I. K., Abbott, P. M., Bigler, M., Blunier, T., Bourne, A. J., Brook, E., Buchardt, S. L., Buzert, C., Clausen, H. B., Cook, E., Dahl-Jensen, D., Davies, S. M., Guillevic, M., Johnsen, S. J., Pedersen, D. S., Popp, T. J., Rasmussen, S. O., Severinghaus, J. P., Svensson, A., and Vinther, B. M.: Consistently dated records from the Greenland GRIP, GISP2 and NGRIP ice cores for the past 104 ka reveal regional millennial-scale $\delta^{18}\text{O}$ gradients with possible Heinrich event imprint, *Quaternary Science Reviews*, 106, 29-46, 10.1016/j.quascirev.2014.10.032, 2014.

Shackleton, N. J., Sánchez-Goñi, M. F., Pailler, D., and Lancelot, Y.: Marine Isotope Substage 5e and the Eemian Interglacial, *Global Planet Change*, 36, 151-155, 10.1016/s0921-8181(02)00181-9, 2003.

675 Toussaint, M. and Bonjean, D. (Eds.): *The Scladina I-4A juvenile Neandertal (Andenne, Belgium). Palaeoanthropology and Context, Etudes et Recherches archéologiques de l'Université de Liège*, 134, ERAUL, Liège, 464 pp., 2014.

Tremaine, D. M., Froelich, P. N., and Wang, Y.: Speleothem calcite farmed in situ: Modern calibration of delta O-18 and delta C-13 paleoclimate proxies in a continuously-monitored natural cave system, *Geochimica Et Cosmochimica Acta*, 75, 4929-4950, 10.1016/j.gca.2011.06.005, 2011.

680 Uemura, R., Kina, Y., Shen, C.-C., and Omine, K.: Experimental evaluation of oxygen isotopic exchange between inclusion water and host calcite in speleothems, *Climate of the Past*, 16, 17-27, 10.5194/cp-16-17-2020, 2020.

van Breukelen, M. R., Vonhof, H. B., Hellstrom, J. C., Wester, W. C. G., and Kroon, D.: Fossil dripwater in stalagmites reveals Holocene temperature and rainfall variation in Amazonia, *Earth and Planetary Science Letters*, 275, 54-60, 10.1016/j.epsl.2008.07.060, 2008.

685 Wainer, K., Genty, D., Blamart, D., Bar-Matthews, M., Quinif, Y., and Plagnes, V.: Millennial climatic instability during penultimate glacial period recorded in a south-western France speleothem, *Palaeogeogr Palaeocl*, 376, 122-131, 10.1016/j.palaeo.2013.02.026, 2013.

Wedepohl, H. K.: The composition of the continental crust, *Geochimica et Cosmochimica Acta*, 59, 1217-1232, 10.1016/0016-7037(95)00038-2, 1995.

Weij, R., Sniderman, J. M. K., Woodhead, J. D., Hellstrom, J. C., Brown, J. R., Drysdale, R. N., Reed, E., Bourne, S., and Gordon, J.: Elevated Southern Hemisphere moisture availability during glacial periods, *Nature*, 626, 319-326, 10.1038/s41586-023-06989-3, 2024.

690 Yang, Q., Scholz, D., Jochum, K. P., Hoffmann, D. L., Stoll, B., Weis, U., Schwager, B., and Andreae, M. O.: Lead isotope variability in speleothems—A promising new proxy for hydrological change? First results from a stalagmite from western Germany, *Chemical Geology*, 396, 143-151, 10.1016/j.chemgeo.2014.12.028, 2015.

